Turing patterns in simplicial complexes

Shupeng Gao,[1,2] Lili Chang,[3,4,*] Matjaž Perc,[5,6,7,8,9] and Zhen Wang[1,2,†]

[1]*School of Mechanical Engineering, Northwestern Polytechnical University, Xi'an 710072, China*
[2]*School of Artificial Intelligence, Optics, and Electronics (iOPEN), Northwestern Polytechnical University, Xi'an 710072, China*
[3]*Complex Systems Research Center, Shanxi University, Taiyuan 030006, China*
[4]*Shanxi Key Laboratory of Mathematical Techniques and Big Data Analysis for Disease Control and Prevention, Taiyuan 030006, China*
[5]*Faculty of Natural Sciences and Mathematics, University of Maribor, Koroška cesta 160, 2000 Maribor, Slovenia*
[6]*Department of Medical Research, China Medical University Hospital, China Medical University, Taichung 404332, Taiwan*
[7]*Alma Mater Europaea, Slovenska ulica 17, 2000 Maribor, Slovenia*
[8]*Complexity Science Hub Vienna, Josefstädterstraße 39, 1080 Vienna, Austria*
[9]*Department of Physics, Kyung Hee University, 26 Kyungheedae-ro, Dongdaemun-gu, Seoul, Republic of Korea*

(Received 18 June 2022; revised 3 November 2022; accepted 6 December 2022; published 27 January 2023)

The spontaneous emergence of patterns in nature, such as stripes and spots, can be mathematically explained by reaction-diffusion systems. These patterns are often referred as Turing patterns to honor the seminal work of Alan Turing in the early 1950s. With the coming of age of network science, and with its related departure from diffusive nearest-neighbor interactions to long-range links between nodes, additional layers of complexity behind pattern formation have been discovered, including irregular spatiotemporal patterns. Here we investigate the formation of Turing patterns in simplicial complexes, where links no longer connect just pairs of nodes but can connect three or more nodes. Such higher-order interactions are emerging as a new frontier in network science, in particular describing group interaction in various sociological and biological systems, so understanding pattern formation under these conditions is of the utmost importance. We show that a canonical reaction-diffusion system defined over a simplicial complex yields Turing patterns that fundamentally differ from patterns observed in traditional networks. For example, we observe a stable distribution of Turing patterns where the fraction of nodes with reactant concentrations above the equilibrium point is exponentially related to the average degree of 2-simplexes, and we uncover parameter regions where Turing patterns will emerge only under higher-order interactions, but not under pairwise interactions.

DOI: 10.1103/PhysRevE.107.014216

I. INTRODUCTION

Patterns are common in nature, from the spots and stripes on the bodies of animals, and the ripples and sand waves in deserts, to the often peculiarly ordered distribution of vegetation in arid regions of the world. These patterns might appear seemingly disordered at first glance, but in fact, it is quite the opposite. They are the product of spontaneous emergence and self-organization that give rise to almost unmatched order and beauty. In 1952, Alan Turing noticed that many of these patterns were far more organized than meets the eye, and he proposed a theory that explained their emergence from fundamental reaction-diffusion processes where different reactants interact and diffuse at different rates, and while doing so create fascinating patterns even from homogeneous, uniform initial states [1].

In fact, Turing's theory provided a general explanation for how different patterns can arise in natural and man-made systems. However, his seminal contributions have not been widely noticed until 1972, when Gierer and Meinhardt, who at the time were still unaware of Turing's work, found that stationary patterns can emerge in certain chemical systems that consist of activators and inhibitors. The activator, as the name suggests, promotes the growth of both the activator's and the inhibitor's density, which, on the contrary, are restrained by the inhibitor. Gierer and Meinhardt also showed that stationary patterns can emerge only when the inhibitor diffuses faster than the activator [2]. After becoming acquainted with Turing's work, Gierer and Meinhardt realized that their findings exactly confirmed Turing's theory. Hence, the 1970s saw the beginning of a growing interest in Turing patterns, which persists today.

Although Turing's theory was originally proposed in the context of chemical systems, it had fruitful applications across disciplines, such as biology [3,4], ecology [5,6], physics [7], ethology [8,9], and engineering [10–14]. Subsequent studies that extended Turing's theory generally branched out into two main categories, whereby one modeled the reaction-diffusion process in the continuous space [15–24], while the other used discrete space to accommodate the reaction-diffusion process [25–32].

Othmer and Scriven were the first to apply Turing's theory in a discrete space medium to generate Turing patterns [31]. In particular, they proposed a reaction-diffusion model where nodes were occupied by reactants and links supported the transfer of these reactants. They found that Turing

*Corresponding author: changll@sxu.edu.cn
†Corresponding author: w-zhen@nwpu.edu.cn

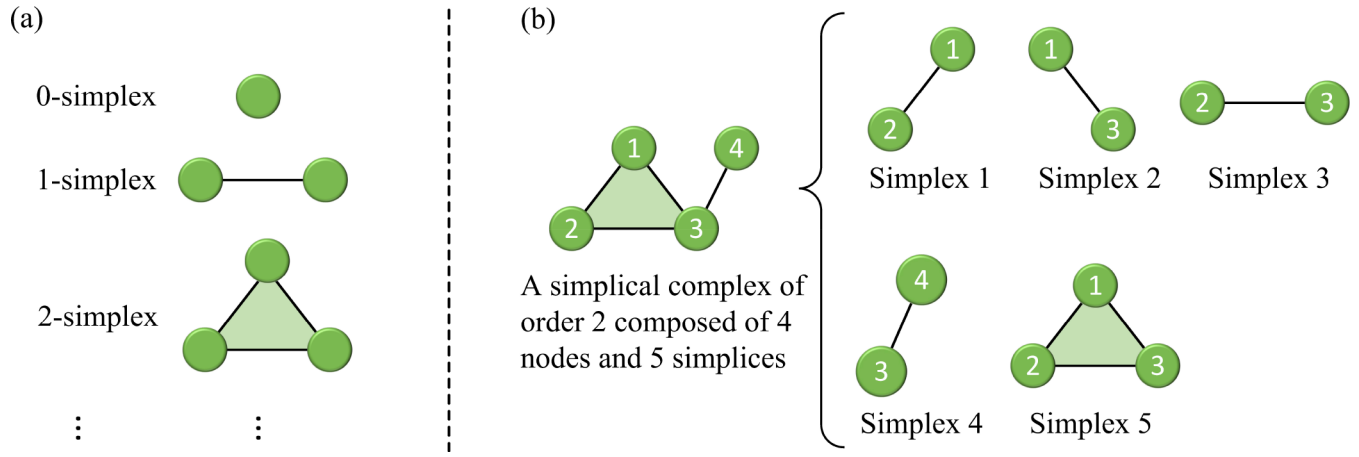

FIG. 1. The simplicial complex model. Panel (a) shows the structure of the fundamental elements, i.e., the d-simplex (for $d = 0, 1, 2,...$), of simplicial complexes. A 0-simplex denotes an isolated node, which cannot participate in the dynamical processes. So the 0-simplex is not considered in this work. When $d > 0$, a d-simplex indicates the connection between $d + 1$ nodes. In other words, A d-simplex has $d + 1$ all-connected nodes. Panel (b) shows an example of a simplicial complex of order $D = 2$ with size $N = 4$ on the left. The order D of a simplicial complex indicates that the dimension of the simplices in it will not exceed D. All simplexes in this simplicial complex are shown on the right. Note that the 2-simplex (1,2,3) and its corresponding 1-simplices (1,2), (1,3), and (2,3) are all taken into account, reflecting the backward compatible characteristic of simplicial complexes.

patterns indeed emerge, and postulated also that they may also arise in other networks, which was later confirmed by many subsequent research efforts [33–35]. Another breakthrough came in 2010, when Nakao and Mikhailov [30] successfully extended Turing's theory from simple networks to large-scale networks, wherein they presented a general mathematical framework that can theoretically derive the Turing instability region of networked reaction-diffusion systems. Subsequent studies then further extended Turing's theory to directed [32], multiplex [36–38], temporal [39,40], and nonnormal networks [41].

However, these previously considered networks were all limited to pairwise links, i.e., having links that connect only two nodes at a time. But recent research has revealed that such networks fail to comprehensively describe group interactions [42–51]. In fact, a paradigm shift in the way we model group interactions is underway and indeed urgent [43,52,53]. Thus the birth of higher-order networks of simplicial complexes, where a single link can connect more than two nodes. Although a simple change in principle, our research will show that this fundamentally affects the emergence of Turing patterns.

In what follows, we propose a reaction-diffusion model embedded in simplicial complexes, where higher-order connections also support the diffusion between patches. More precisely, our model enables the transfer flux per unit time is related not just to pairwise connections, but also to higher-order connections. We will show that, as a consequence, Turing patterns can sometimes emerge spontaneously only if higher-order connections are enabled, but not in the corresponding reduced "standard" network with just pairwise links. We will also show that the statistical characteristic of the stable distribution of the activator is exponentially correlated to the average degree of higher-order connections, in turn indicating a strong interrelation between Turing patterns and higher-order connections.

II. MATHEMATICAL MODEL

A. Simplicial complexes

Let us consider a simplicial complex $S(V, E)$ of order D, where $V = \{1, \ldots, N\}$ indicates the collection of N nodes and $E = \{E_1, \ldots, E_M\}$ denotes the set of M simplices. Each simplex $E_m (m \in \{1, \ldots, M\})$ contains an unordered collection of all-connected $|E_m|$ nodes with $d_m = |E_m| - 1 \leqslant D$, where $|E_m|$ is the size of simplex E_m (the number of nodes involved) and d_m denotes its order. The order of a simplicial complex equals the largest order of all simplices in it, as shown by $D = \max\{d_m, m = 1, \ldots, M\}$.

The structure of simplices is depicted intuitively in Fig. 1. Several properties are worth mentioning. First, all nodes in the same simplex are linked. Second, the simplex m represents a group connection when $|E_m| > 2$ and reduce to a "standard" edge with a pairwise connection when $|E_m| = 2$, and a simplicial complex will reduce to a "standard" network when $|E_m| = 2$ for $\forall\ m$. Third, simplicies are backward compatible, which means that a simplex of order d $(d > 0)$ contains simplicies of dimension d', where $d' = d - 1, \ldots, 0$. This compatibility is opposed to the cases in hypergraph structures [46]. Hereafter, the simplex of order d is referred to as a d-simplex for convenience.

We then move to define the adjacent matrix of a simplicial complex. First, let us introduce the incidence matrix $\boldsymbol{B}$ of $N \times M$ dimesion, whose element B_{im} indicates whether node i belongs to simplex m,

$$B_{im} = \begin{cases} 1 & \text{for } i \in E_m, \\ 0 & \text{otherwise.} \end{cases} \tag{1}$$

It is of note that "standard" networks also have the same matrix. However, in the incidence matrix of a "standard" network, the number of nonzero elements in each column is the same, i.e., two, because only pairwise connections between

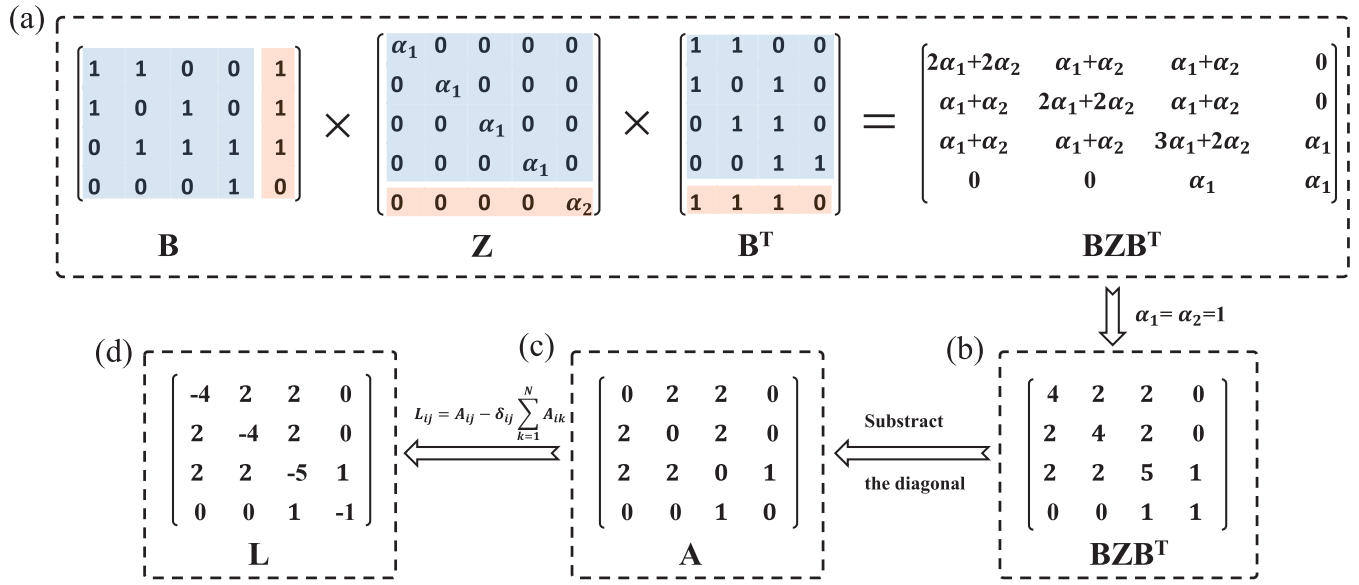

FIG. 2. An illustration of how a simplicial complex's adjacent matrix is built. The general mathematical calculation of the adjacent matrix A is given in Eq. (3). Here the simplicial complex in Fig. 1(b) is taken as an example to explicitly show how its adjacent matrix is constructed. Panel (a) displays the matrices $\mathbf{B}$, $\mathbf{Z}$, and $\mathbf{B}^T$ of the simplicial complex and computes the result of $\mathbf{BZB}^T$. The simplicial complex in Fig. 1(b) is composed of four nodes and five simplices (four simplices of order 1 and one simplex of order 2). Therefore, the matrix $\mathbf{B}$ is of 4×5 dimension, and $\mathbf{Z}$ is of 5×5 dimension. In matrices $\mathbf{B}$, $\mathbf{Z}$, and $\mathbf{B}^T$, the light blue shadow covers the elements that correspond to the simplices of order 1, while the light yellow shadow covers the elements that are dominated by the simplex of order 2. α_1 and α_2 indicate the simplex strength of order 1 and order 2, respectively. For simplicity, we set $\alpha_1 = \alpha_2 = 1$ and then we get the concrete value of $\mathbf{BZB}^T$ in panel (b). Panel (c) then shows the adjacent matrix A as defined by $\mathbf{A} = \mathbf{BZB}^T - \mathrm{diag}(\mathbf{BZB}^T)$. Finally, panel (d) shows the Laplacian matrix L based on the adjacent matrix using $L_{ij} = A_{ij} - \delta_{ij}\sum_{k=1}^{N} A_{ik}$.

two nodes are considered. While in a simplicial complex's incidence matrix, each column can have more than two nonzero entries, because the simplicial complex takes into account the group connection of multiple nodes. Second, once the incidence matrix $\boldsymbol{B}$ has been defined, we can construct an $M\times M$ matrix $\boldsymbol{C} = \boldsymbol{B}^T\boldsymbol{B}$, with the entry C_{mn} indicating the number of nodes in $E_m \cap E_n$. The entry C_{mm} on the diagonal equals $|E_m|$, which counts the number of nodes in the simplex E_m. Furthermore, d_m, the dimension of the simplex E_m, can be calculated through $d_m = |E_m| - 1 = C_{mm} - 1$. Third, to portray the relationship between nodes, we introduce the parameter α_d $(d = 1, \ldots, D)$, the d-simplex strength, which measures the extent to which a d-simplex contributes to the connection between the nodes in it.

As a result of the preceding definitions, the connection between node i and j can be described as

$$A_{ij} = \begin{cases} \sum_{m=1}^{M} B_{im} B_{jm} \alpha_{d_m} & \text{for } i \neq j, \\ 0 & \text{for } i = j, \end{cases} \tag{2}$$

where $d_m \in [1, D]$ indicates the order of the simplex E_m. M denotes the number of simplices in the simplicial complex. Then we can get the adjacent matrix $\boldsymbol{A}$ of a simplicial complex by rewriting Eq. (2) into the matrix form

$$\boldsymbol{A} = \boldsymbol{BZB}^T - \mathrm{Diag}(\boldsymbol{BZB}^T), \tag{3}$$

where $\boldsymbol{B}$ denotes the incidence matrix of $N\times M$ dimension. $\boldsymbol{Z}$ is a diagonal matrix of $M\times M$ dimension:

$$\boldsymbol{Z} = \begin{pmatrix} \alpha_{d_1} & & \\ & \ddots & \\ & & \alpha_{d_M} \end{pmatrix}. \tag{4}$$

The operator symbol $\mathrm{Diag}(\boldsymbol{X})$ denotes the extraction of the diagonal entries of the square matrix $\boldsymbol{X}$ as a new diagonal matrix. Because the main diagonal of the adjacency matrix is generally set to 0, the latter term $\mathrm{Diag}(\boldsymbol{BZB}^T)$ in Eq. (3) is subtracted.

B. Reaction-diffusion systems in simplicial complexes

After constructing the adjacent matrix $\boldsymbol{A}$, we introduce the reaction-diffusion system on simplicial complexes. The system can be depicted by a set of ordinary differential equations (ODEs). Each equation contains two terms: the local reaction within the node and the diffusion between nodes. These terms characterize different dynamical kernels that contribute to the change in specie density.

In a two-species (activator u and inhibitor v) system, the local dynamics in node i are generally described by two nonlinear functions $f(u_i, v_i)$ and $g(u_i, v_i)$, where u_i and v_i denote the activator and inhibitor densities in node i, respectively. According to Ficks' law, the change of u_i per unit time caused by diffusion is proportional to $\sum_{j=1}^{N} A_{ij}(u_j - u_i) = \sum_{j=1}^{N} L_{ij}u_j$. $\boldsymbol{L}$ represents the Laplacian matrix of the adjacent matrix $\boldsymbol{A}$. $L_{ij} = A_{ij} - \delta_{ij}\sum_{k=1}^{N} A_{ik}$, where δ_{ij} denotes the

Kronecker delta, $\delta_{ij} = 1$ if and only if $i = j$, otherwise $\delta_{ij} = 0$. Similarly, the change of v_i per unit time caused by diffusion is proportional to $\sum_{j=1}^{N} L_{ij} v_j$. The Laplacian matrix $\mathbf{L}$ is computed simply based on the adjacent matrix $\mathbf{A}$. Although the general construction of a simplicial complex's adjacent matrix $\mathbf{A}$ is mathematically shown in Sec. II A, an intuitive illustration of the building process of a specific simplicial complex's adjacent matrix is still required. Therefore, Fig. 2 explicitly shows how we construct the adjacent matrix $\mathbf{A}$ and corresponding Laplacian matrix $\mathbf{L}$ of the simplicial complex shown in Fig. 1(b).

Therefore, the reaction-diffusion system organized in simplicial complexes can be depicted by the following ODEs:

$$\begin{aligned} \frac{du_i}{dt} &= f(u_i, v_i) + \varepsilon \sum_{j=1}^{N} L_{ij} u_j, \\ \frac{dv_i}{dt} &= g(u_i, v_i) + \sigma\varepsilon \sum_{j=1}^{N} L_{ij} v_j, \end{aligned} \tag{5}$$

where ε and $\sigma\varepsilon$ denote the diffusional mobilities of activator and inhibitor, respectively, and σ indicates the ratio between them.

There is no discernible difference between the mathematical expressions of the reaction-diffusion system in a "standard" network and a simplicial complex. However, the outcomes of the systems in these two structures differ due to the distinct Laplacian matrices, which will be discussed in detail in the following section.

III. RESULTS

A. Setup of simulations

To investigate how simplicial complexes influence the formation of Turing patterns in reaction-diffusion systems, we carry on several simulations. This subsection introduces the preliminary work, including the generation of simplicial complexes, the configuration of dynamical models, and initial conditions for simulations.

1. The simplicial complex generation

Without loss of generality, the simplicial complexes we use are all of order 2, which means that pairwise connections (1-simplices) and three-node group connections (2-simplices) are taken into account. As a crucial characteristic of simplicial complexes, the average degree of order d is usually utilized to distinguish various simplicial complexes and is defined as

$$\langle k^{(d)} \rangle = n_d \frac{(d+1)}{N}, \tag{6}$$

where $\langle k^{(d)} \rangle$ denotes the average degree of order d, n_d indicates the number of d-simplices, and N is the number of nodes in the simplicial complex. The efficient degree-adjustable algorithm proposed in Ref. [42] is used to generate the simplicial complex. As shown below, the algorithm goes through two stages to generate a simplicial complex of order $D = 2$. Given a set V of N nodes, we first construct pairwise connections (1-simplices) for any $i, j \in V$ with probability $p^{(1)}$. At this stage, the number of generated 1-simplices is approximately $\frac{N(N-1)}{2} p^{(1)}$. Therefore, the current average degree of order 1 approximately equals $\frac{N(N-1)}{2} p^{(1)} \frac{1+1}{N} = (N-1)p^{(1)}$. Then, we construct three-node group connections (2-simplices) for any $i, j, k \in V$ with probability $p^{(2)}$. At this point, there are approximately $\frac{N(N-1)(N-2)}{6} p^{(2)}$ 2-simplices generated. So the average degree of order 2, i.e., $\langle k^{(2)} \rangle$, is approximately $\frac{N(N-1)(n-2)}{6} p^{(2)} \frac{2+1}{N} = \frac{(N-1)(N-2)}{2} p^{(2)}$. It is of note that the second stage of constructing 2-simplices also contributes to the increase of the average degree of order 1. The specific contribution can be calculated by taking into account the various possibilities for attaching a 2-simplex (i, j, k) to a node i. Specifically, the 1-order degree of node i increases by 2 for the construction of each 2-simplex (i, j, k) when neither the 1-simplex (i, j) nor the 1-simplex (i, k) is constructed during the first stage; the probability of this scenario is $(1 - p^{(1)})^2$. Similarly, the construction of each 2-simplex (i, j, k) increases the 1-order degree of node i by 1 with probability $p^{(1)}(1 - p^{(1)})$ when either the 1-simplex (i, j) exists during the first stage but the 1-simplex (i, k) not, or vice versa. Each of these two cases has the same probability to happen. So the contribution of these two cases is $2p^{(1)}(1 - p^{(1)})$. Considering all possible scenarios, the overall contribution of each 2-simplex to the increase of the 1-order of node i is $2(1 - p^{(1)})$. Therefore, adding together the two contributions made by 1-simplices and 2-simplices, the expected average degree of order 1, i.e., $\langle k^{(1)} \rangle$, can be calculated as $\langle k^{(1)} \rangle \approx (N-1)p^{(1)} + 2\langle k^{(2)} \rangle (1 - p^{(1)})$. We can therefore construct simplicial complexes with desired $\langle k^{(1)} \rangle$ and $\langle k^{(2)} \rangle$ by adaptively calculating the values of $p^{(1)}$ and $p^{(2)}$ as

$$\begin{aligned} p^{(1)} &= \frac{\langle k^{(1)} \rangle - 2\langle k^{(2)} \rangle}{(N-1) - 2\langle k^{(2)} \rangle}, \\ p^{(2)} &= \frac{2\langle k^{(2)} \rangle}{(N-1)(N-2)}. \end{aligned} \tag{7}$$

One can refer to Methods in Ref. [42] for more details.

2. Dynamical model reaction kernels and parameter configurations

Here, we introduce the dynamical model used in the reaction-diffusion system (5). We choose three paradigmatic models ranging from biology to physics to provide a comprehensive view of Turing pattern formation in simplicial complexes. The following are the nonlinear functions and detailed information.

(a) Gierer-Meinhardt (GM) model [2]: The GM model was first proposed to model the chemical dynamics in cellular, which well explained the pattern formation in morphogenesis. Its nonlinear reaction terms are as follows:

$$\begin{aligned} f(u, v) &= \frac{u^2}{v} - au, \\ g(u, v) &= bu^2 - cv. \end{aligned} \tag{8}$$

Through all simulations, the parameters are fixed to $a = 1$, $b = 9$, $c = 3$, $\varepsilon = 0.01$, $\sigma = 100$.

(b) Leslie-Gower-Holling (LG) model: Leslie and Gower proposed a two-species model that characterize the interaction between predator and prey populations [54]. Studies show that the LG model has rich dynamics, from which diverse patterns

can spontaneously arise [55,56]. The reaction terms of the LG model are as follows:

$$f(u, v) = u(1-u) - \frac{u^2 v}{au^2+1},$$
$$g(u, v) = bv\left(1 - \frac{cv}{u}\right). \tag{9}$$

We set the parameters to $a = 80$, $b = 0.6$, $c = 0.01568$, $\varepsilon = 0.0015$, $\sigma = 120$ for all simulations.

(c) FitzHugh-Nagumo (FHN) model: In 1961 FitzHugh proposed a set of nonlinear differential equations that described the periodic oscillations of neuronal action potentials in response to suprathreshold norm current stimulation [57]. In the next year, Nagumo *et al.* proposed a mathematically equivalent circuit model to FitzHugh's equations, revealing the mechanism of action potential generation and conduction in the giant axons of the gunny squid [58]. Their pioneering model is often investigated [59,60] and referred to as the FHN model, whose reaction terms are

$$f(u, v) = c\left(u - \frac{u^3}{3} - v\right),$$
$$g(u, v) = c(au - bv). \tag{10}$$

The parameters are set to $a = 3$, $b = 2$, $c = 1$, $\varepsilon = 0.01$, $\sigma = 15$.

3. The initial condition for numerical simulations

During the numerical simulations, we need to add small perturbations around the equilibrium for initialization. When all of the settings satisfy the requirement of Turing instability, the perturbations will grow exponentially and the system will reach a new heterogeneous stable state, appearing as Turing patterns. Otherwise, the perturbations will fade away and the system will return back to the homogeneous equilibrium. For all simulations, we define the initial condition with perturbations as follows:

$$u_i(0) = u^e + \eta_i',$$
$$v_i(0) = v^e + \eta_i'', \tag{11}$$

where $\eta_i', \eta_i'' \sim \mathcal{N}(0, 0.0001)$.

B. Turing patterns mediated by higher-order connections

Topology plays a vital role in the formation of Turing patterns. According to a recent study, the Turing instability condition is related to topological properties. Turing patterns can emerge spontaneously only when the topology's Laplacian has eigenvalues located in the instability region $(\Lambda^*, \Lambda^{**})$ (see Appendix A). Λ^* and Λ^{**} denote the boundaries between which eigenvalues satisfy the Turing instability condition [29].

Originating from the relationship between Laplacian's eigenvalues and Turing instabilities, we furthermore investigate how higher-order connections in simplicial complexes affect the formation of Turing patterns. Let us first consider a simplicial complex with 100 vertices of order 2. We set $\alpha_1 = 1$ and vary the value of α_2 to see how the domain of Laplacian's eigenvalues changes. Figure 3 shows that when

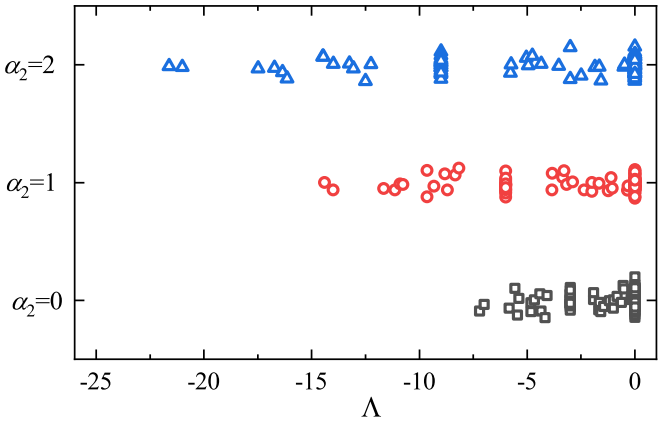

FIG. 3. The distribution of Laplacian eigenvalues Λ of a two-dimensional simplicial complex with varying 2-simplex strength α_2. The simplicial complex contains 100 vertices with $\langle k^{(1)} \rangle = 1.38$ and $\langle k^{(2)} \rangle = 0.69$. The 1-simplex strength α_1 is fixed to 1, and the 2-simplex strength α_2 is set to 0, 1 and 2. When $\alpha_2 = 0$, the simplicial complex is a "standard" network with pairwise connections. When $\alpha_2 > 0$, the higher-order connections, i.e., three-body group connections, are considered. As α_2 increases, the domain of the distribution of Laplacian eigenvalues becomes wider.

$\alpha_2 = 0$, where the simplicial complex reduces to a standard network, the eigenvalues are tightly distributed and narrow in range. Moreover, the width of the eigenvalues' range of the Laplacian matrix appears to have a positive correlation with α_2, i.e., as α_2 increases, the Laplacian has wider eigenvalue's ranges.

This phenomenon implies that there may be a situation where Turing patterns can only emerge in the simplicial complex when higher-order connections are considered ($\alpha_2 > 0$). To explore such a situation, we perform numerical calculations for the GM, LG, and FHN models in the same simplicial complex used in Fig. 3. We also fix α_1 to 1 and vary the value of α_2 during the simulations.

Figure 4 shows the Laplacian eigenvalue distributions of the simplicial complex (with different 2-simplex strengths) on the dispersion curve (GM model) on the first row and corresponding patterns on the second row. The dispersion curve λ is calculated through the Turing instability analysis (see Appendix A). Turing patterns will spontaneously arise only when there are Laplacian eigenvalues Λ that satisfy $\lambda(\Lambda) > 0$. Figure 4(a) shows that there are no eigenvalues that satisfy $\lambda(\Lambda) > 0$, and the corresponding stable distribution of u_i shown in Fig. 4(d) are homogeneous, i.e., no Turing patterns. Interestingly, when $\alpha > 0$, such as $\alpha = 1, 2$, the eigenvalue distributions meet the Turing instability requirement that $\exists\Lambda$, $\lambda(\Lambda) > 0$ [Figs. 4(b) and 4(c)], and the system reaches new heterogeneous stable states, i.e., Turing patterns [Figs. 4(e) and 4(f)]. It is interesting that patterns develop only on a subset of nodes in Fig. 4. This may be due to the fact that only a subset of values is nonzero in the critical eigenvectors which correspond to the unstable eigenvalues [the abscissa of the red points in Figs. 4(b) and 4(e)] of the Laplacian matrices. Because the growth of the initial perturbations is linearly related to the critical eigenvectors as shown in Eq. (A3) in the Appendixes. The perturbations will grow only on nodes

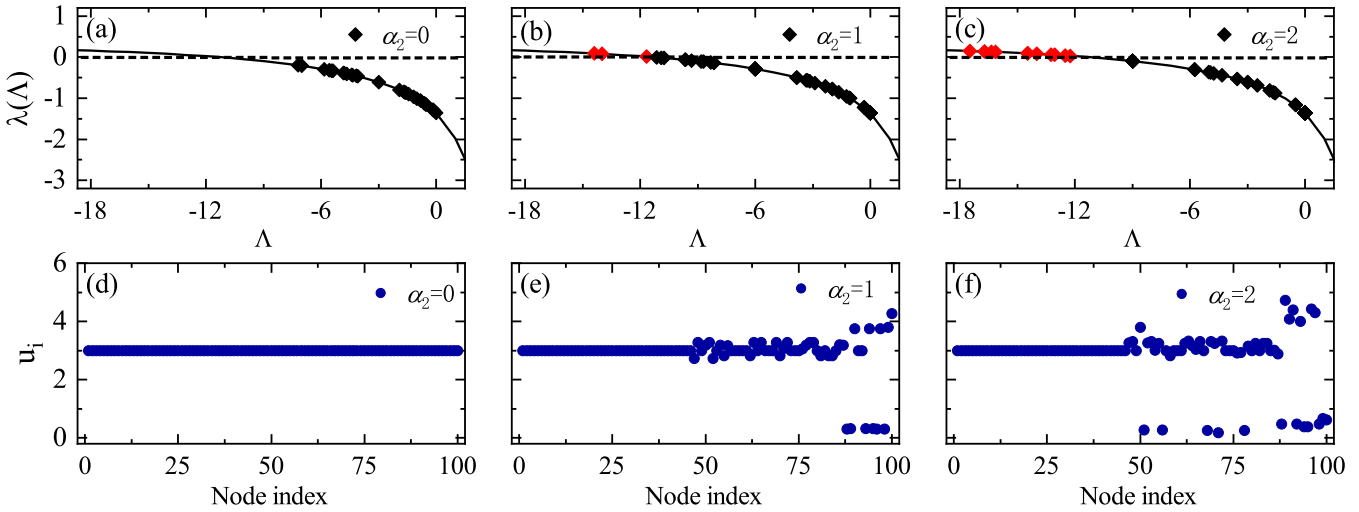

FIG. 4. Turing patterns induced by three-body connections (2-simplices) for GM model. Panels (a), (b), and (c), respectively, show the dispersion relationship between the system growth factor λ and Laplacian eigenvalue Λ for $\alpha_2 = 0$, 1, and 2. The simplicial complex used here is the same as the one used in Fig. 3. The 1-simplex strength α_1 is fixed to 1. The dispersion curve is calculated through Turing instability analysis (see Appendix A). Turing patterns will arise only if Laplacian eigenvalues meet the condition that $\exists\Lambda, \lambda(\Lambda) > 0$. Panels (d), (e), and (f) respectively present the corresponding distributions of u_i after numerical calculations for $\alpha_2 = 0$, 1, and 2. $\alpha_2 = 0$ implies that the simplicial complex returns to a "standard" network. When $\alpha_2 = 0$, the Turing instability condition is not satisfied (a), resulting in a homogeneous distribution of u_i (d). Interestingly, when $\alpha_2 > 0$, such as $\alpha_2 = 1$, 2, the three-body connections are taken into account, and the Turing instability condition is satisfied as shown in panels (b) and (c). The dispersion points that meet the instability requirement are colored in red in panels (b) and (c). Panels (e) and (f) then exhibit the corresponding distributions of u_i as Turing patterns for $\alpha_2 = 1$, 2. In this case, Turing patterns can only spontaneously when $\alpha_2 > 0$. Therefore, it can be inferred that Turing patterns can be induced by three-body connections in the simplicial complex.

whose corresponding values in the critical eigenvectors are nonzero and will fade away on those with zero values in the critical eigenvectors. Turing patterns, therefore, can develop only on nodes where the initial perturbations can grow over time. One can turn to Fig. 8 in the Appendixes for more information on the value distribution of critical eigenvectors.

Similar phenomena to that shown in Fig. 4 are also found in the LG and FHN models (see Figs. 9 and 10 in the Appendixes). Therefore, in this case, Turing patterns are induced by the higher-order connections in the simplicial complex, which are similar to the case in hypergraphs [46].

In the pioneering work on investigating Turing patterns on networked reaction-diffusion systems, Nakao and Mikhailov found that the outcome of the system's evolution is quite sensitive to the initial conditions and revealed the multistabilities of the system [30]. Here we found such multistabilities still hold on reaction-diffusion systems organized in simplicial complexes. Figure 5 shows how Turing patterns' amplitude, calculated as amplitude $= \{\sum_{i=1}^{N}[(u_i - u^e)^2 + (v_i - v^e)^2]\}^{\frac{1}{2}}$, changes when the 2-simplex strength α_2 is gradually changed in either an upward or downward direction for the GM model. The value of α_2 reflects the strength of three-body connections and indicates how important the 2-simplices are in the simplicial complex. We start by gradually increasing the 2-simplex strength α_2 from $\alpha_2 = 0$. The amplitude undergoes a sudden jump from 0 to a high value at $\alpha_2 \cong 1$, implying the arising of Turing instability. This sudden jump explains the finding in Fig. 4 that three-body connections can induce Turing instability. As α_2 is further increased to 2, the amplitude grows

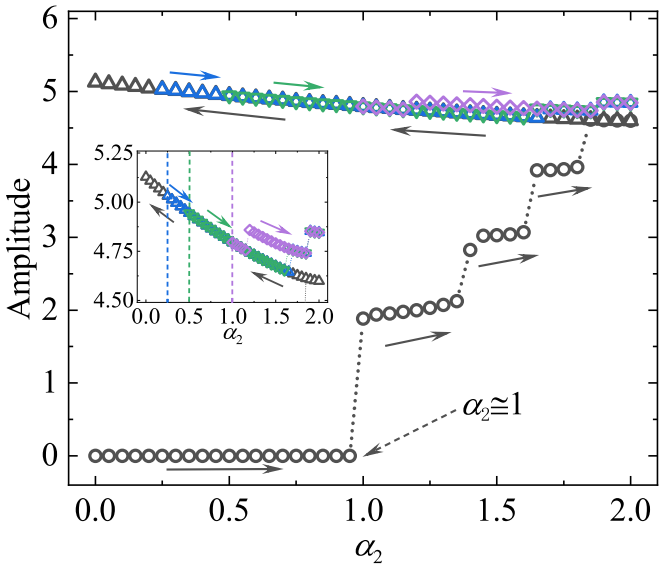

FIG. 5. Multistabilities of the GM model on simplicial complexes. The amplitude of the solutions under varying α_2 in either an upward or downward direction is plotted vs the 2-simplex strength α_2. Starting to increase α_2 from 0 with the initial condition (11), the amplitude goes through a sudden jump from 0 at $\alpha_2 \cong 1$. Further changing the value of α_2, the coexistence of multiple stable solutions can be observed. The changing direction of α_2 is directed by arrows. The inset zooms the amplitude scale into a narrow one, i.e., [4.5,5.25], for a better view. The simplicial complex used here is the same as the one used in Figs. 3 and 4.

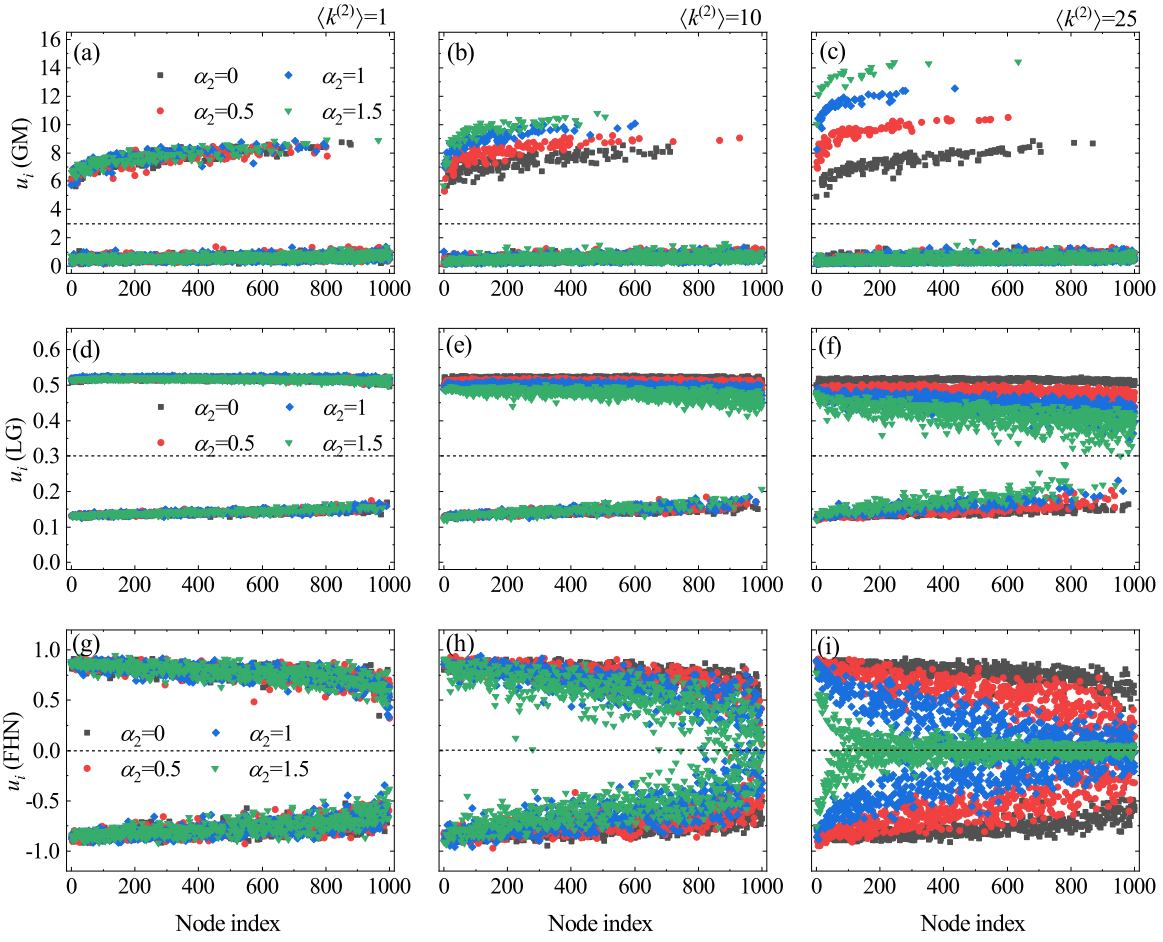

FIG. 6. Spontaneously arising Turing patterns in simplicial complexes of order 2 with different average degrees of order 2 $\langle k^{(2)}\rangle$. The Turing patterns, i.e., the stable distribution of u_i, of the GM, LG, and FHN models are shown in the first, second, and third rows, respectively. While the first, second, and third columns show the results in the simplicial complex with $\langle k^{(2)}\rangle = 1$, 10 and 25, respectively. In each panel, the dashed black line represents the equilibrium u^e. From panel (a) to panel (c) (the GM model), the number of points above the equilibrium decreases as $\langle k^{(2)}\rangle$ increases. From panel (d) to panel (f) (the LG model), the points below the equilibrium have the trend to move up and the number of points above the equilibrium appears to increase as $\langle k^{(2)}\rangle$ increases. From panel (g) to panel (i) (the FHN model), the number of points near the equilibrium appears to increase as $\langle k^{(2)}\rangle$ increases. Considering these phenomena together, we may infer that the structure of Turing patterns, i.e., the stable distribution of u_i, may be correlated to the average degree of order 2. Here the simplicial complexes of order 2 are generated according to the algorithm in Sec. III A. For comparability, we set that all simplexes comprise 1000 nodes and have the same average degree of order 1, i.e., $\langle k^{(1)}\rangle = 50$.

and will go through several sudden jumps. Decreasing α_2 at $\alpha_2 = 2$, the amplitude does not decrease but instead continuously increases. Reversing the changing direction of α_2 during the decreasing process of α_2 at three points ($\alpha_2 = 0.25$, $\alpha_2 = 0.5$, and $\alpha_2 = 1$), we further observe multiple stable solutions coexisting in the system. Such multistabilities are also found in the LG and FHN models; one can refer to Fig. 11 in the Appendixes for more information.

C. Correlations between the structure of Turing patterns and the average degree of higher-order connections

This study focuses on Turing patterns on simplicial complexes, which differs from the conventional subjects in that the underlying structure contains higher-order connections. The impact of higher-order connections on the Turing patterns is then naturally focused on. The preceding subsection discusses the effect of the existence and strength of three-body connections (2-simplex) on the formation of Turing patterns in a simplicial complex of order 2. In this subsection, we will look at how the density of higher-order connections, i.e., the average degree of higher order, affects the formation of Turing patterns.

We generate several random simplicial complexes of order 2 with 1000 nodes using the algorithm introduced in Sec. II. These simplicial complexes differ in terms of $\langle k^{(2)}\rangle$, which ranges from 1 to 25, but they all have the same $\langle k^{(1)}\rangle = 50$ for comparability. In these simplicial complexes, we perform numerical calculations for the GM, LG, and FHN models. Some typical patterns (the stable distribution of u_i) obtained by one single trial are shown in Fig. 6, where the black dashed line indicates the equilibrium u^e for each model. The first row of Fig. 6 shows the results of the GM model, where we can find that as $\langle k^{(2)}\rangle$ increases, fewer points are located above the equilibrium, and this trend strengthens as α_2 increases. The

TABLE I. The detailed information for the nonlinear regression fitting curves for numerical results in Figs. 7(a), 7(b), and 7(c).

Model	α_2	$r_1 \in$ CI(99%)	$r_2 \in$ CI(99%)	$r_3 \in$ CI(99%)	R^2
GM	0	0.7327	−0.58885	−6.67346E-4	0.93256
	0.5	0.00414	0.14053	−0.02205	0.99655
	1	0.01546	0.1309	−0.05082	0.99848
	1.5	0.01018	0.13593	−0.06906	0.99933
LG	0	0.71042	−0.00258	−0.15871	0.27254
	0.5	0.80597	−0.09659	−0.01773	0.99046
	1	0.79036	−0.0834	−0.04626	0.99582
	1.5	0.78226	−0.07597	−0.08259	0.9964
FHN	0	−0.04956	0.04956	1.80228E-4	0.55505
	0.5	−0.00315	0.00207	0.11316	0.99349
	1	−0.01505	0.00948	0.12675	0.99579
	1.5	−0.03052	0.01629	0.15755	0.99562

results of the LG model are shown in the second row of Fig. 6. As $\langle k^{(2)}\rangle$ increases, the points located under the equilibrium tend to be closer to the equilibrium, and the number of points presented under the equilibrium decreases. The third row of Fig. 6 shows the results of the FHN model. Unlike the GM and LG models, the number of points on either side of the equilibrium appears not to change as $\langle k^{(2)}\rangle$ increases, but the number of points near the equilibrium point is increasing.

We infer from such phenomena that some statistical features of Turing patterns may be related to $\langle k^{(2)}\rangle$. To reveal potential relationships, we propose the metric P^M, which measures the fraction of the nodes that have density within the range $[u^e - 0.1, u^e + 0.1]$ for the FHN model,

$$P^M = \left\{ 2N - \sum_{i=1}^{N} |\mathrm{sgn}(u_i - u^e - 0.1) + \mathrm{sgn}(u_i - u^e + 0.1)| \right\} \Big/ (2N), \tag{12}$$

and define P^T, which measures the fraction of the nodes with higher density than equilibrium u^e for the GM and LG models,

$$P^T = \frac{\sum_{i=1}^{N} \mathrm{sgn}'(u_i - u^e)}{N}, \tag{13}$$

where $\mathrm{sgn}(x)$ and $\mathrm{sgn}'(x)$ are the sign function and modified sign function, respectively,

$$\mathrm{sgn}(x) = \begin{cases} 1 & \text{for } x > 0, \\ 0 & \text{for } x = 0, \\ -1 & \text{for } x < 0, \end{cases} \tag{14}$$

$$\mathrm{sgn}'(x) = \begin{cases} 1 & \text{for } x > 0, \\ 0 & \text{for } x \leqslant 0. \end{cases} \tag{15}$$

As mentioned, the system has multistabilities. To mitigate the influence of such multistabilities, we increase the number of trials to 25 by repeating experiments. Specifically, for each parameter setting, we repeat the calculations on five different networks (with the same degree of both order 1 and order 2 for consistency) with five different initial conditions. Figures 7(a), 7(b), and 7(c) then plot the scatter diagrams of the averaged values of P^T and P^M in regard to varying $\langle k^{(2)}\rangle$ obtained by numerical simulations. When $\alpha_2 = 0$, the simplicial complex contains only pairwise connections, which is in accordance with a "standard" network. In this case $\langle k^{(2)}\rangle$ barely influence the value of P^T (for the GM and LG models) and P^M (for the FHN model). However, when $\alpha_2 > 0$, the correlation between these metrics and $\langle k^{(2)}\rangle$ gradually appears. For example, P^T will decrease as $\langle k^{(2)}\rangle$ increases for the GM model. While P^T will increase as α_2 increases for the LG model. For the FHN model, P^M will increase in an accelerated manner as $\langle k^{(2)}\rangle$ increases. Moreover, all these correlations for the GM, LG, and FHN models will be enhanced as α_2 increases. Following the powerful theory proposed in [30], we further calculate the theoretical predictions to support these findings in numerical simulations using the mean-field analysis (see Appendix C for more information). The theoretical results for the GM [Fig. 7(d)] and LG [Fig. 7(e)] models are in great agreement with their corresponding simulation results [Figs. 7(a) and 7(c)]. The FHN model's theoretical [Fig. 7(f)] and simulation [Fig. 7(c)] results both exhibit strong correlations between P^M and $\langle k^{(2)}\rangle$, though they differ in terms of the exact values of P^M.

To gain a better understanding of such correlations, we attempted to fit them with the exponential model

$$\hat{P} = r_1 + r_2 e^{r_3 \langle k^{(2)}\rangle}. \tag{16}$$

The lines in Fig. 7 indicate the fitting curves obtained from nonlinear regressions. The fitting appears to be successful for both theoretical and numerical results. It is of note that many other nonlinear functions may also well fit the data, and they are all practicable in our work. For simplicity, we herein chose a simple function, i.e., the exponential function (16), to quantitatively verify the correlation between the structure of Turing patterns on simplicial complexes and $\langle k^{(2)}\rangle$ of simplicial complexes. The quantitative information of the fitting is shown in Tables I (for numerical results) and II (for results obtained by mean-field analysis) in the Appendixes. In detail, the estimated parameters are r_1, r_2, and r_3 in Eq. (16). The coefficient of determination R^2 is also calculated to describe the goodness of the exponential fitting. Compared to the situation where $\alpha_2 = 0$, when $\alpha_2 > 0$, R^2 has much higher value, and nearly holds beyond 0.97 in all three models in the regression of both theoretical and numerical results. Such

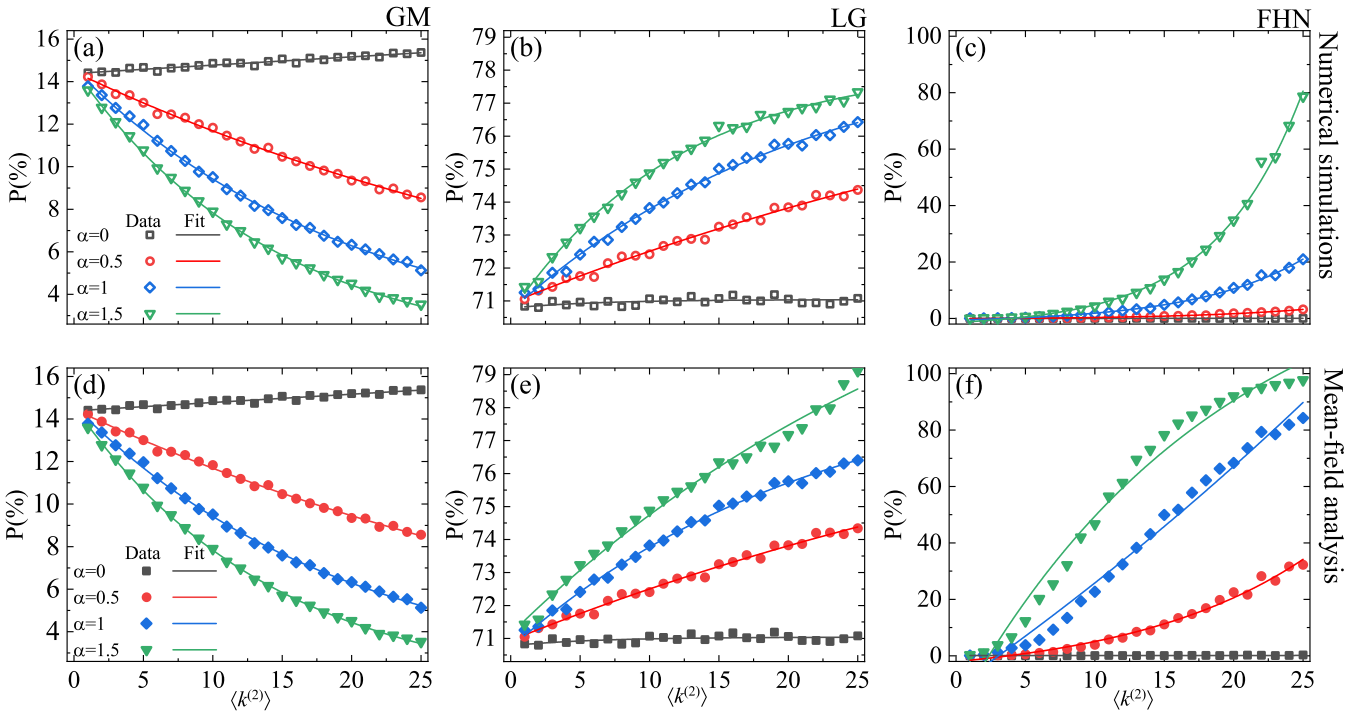

FIG. 7. The correlation between the proposed statistical indicators of Turing patterns and the average degree of order 2. The first row [panels (a), (b), and (c)] and the second row [panels (d), (e), and (f)] are obtained by numerical simulations and mean-field analysis, respectively. Hollow dots and solid dots represent the data obtained by numerical simulations and mean-field analysis, respectively. While lines indicate the exponential fitting cure obtained by nonlinear regression. The detailed information of the fitting is shown in Tables I (for numerical simulations) and II (for mean-field analysis) in the Appendixes. In terms of simulations results, panels (a) and (b) show the relation between P^T and $\langle k^{(2)}\rangle$ for the GM and LG models, respectively. Panel (c) shows the relation between P^M and $\langle k^{(2)}\rangle$ for the FHN model. Intuitively, when $\alpha_2 > 0$, the data are fitted successfully for all these three models, implying underlying correlations between the average degree of order 2 ($\langle k^{(2)}\rangle$) and the statistical indicators of Turing patterns (P^T and P^M). P^T and P^M, on the other hand, reflect the stable distribution of u_i, i.e., the structure of Turing patterns. Therefore, it is reasonable to conclude that the average degree of order 2 has an obvious correlation with the structure of Turing patterns. Such phenomena observed from numerical simulations are further validated by mean-field analysis. Specifically, panels (d) and (e) show the results obtained by mean-field analysis for the GM and LG models, respectively, and are in a good agreement with the simulation results in panels (a) and (b). The FHN model's mean-field analysis results and simulation results both exhibit strong correlations between P^M and $\langle k^{(2)}\rangle$, though they differ in terms of the exact values of P^M. The simplicial complexes of order 2 used here are generated using the algorithm introduced in Sec. III A. To ensure comparability, we set that all simplexes comprise 1000 nodes and have the same average degree of order 1 $\langle k^{(1)}\rangle = 50$.

values of R^2 are significantly close to 1, and therefore, indicate perfect fittings for both theoretical and numerical results when $\alpha_2 > 0$.

In brief, when higher-order connections are considered ($\alpha_2 > 0$), it can be seen that the average degree of higher-order connections has strong correlations with the structure of

TABLE II. The detailed information for the nonlinear regression fitting curves for theoretical results in Figs. 7(d), 7(e), and 7(f).

Model	α_2	$r_1 \in$ CI(99%)	$r_2 \in$ CI(99%)	$r_3 \in$ CI(99%)	R^2
GM	0	0.75531	−0.61146	−6.44407E-4	0.9325
	0.5	0.00424	0.14043	−0.02208	0.99651
	1	0.01546	0.1309	−0.05082	0.99848
	1.5	0.01018	0.13593	−0.06906	0.99933
LG	0	0.71041	−0.0026	−0.15985	0.27748
	0.5	0.80569	−0.0963	−0.01769	0.99026
	1	0.79119	−0.08412	−0.04531	0.99595
	1.5	0.85823	−0.14685	−0.02818	0.98798
FHN	0	8.85211E-4	3.85103E-40	3.37722	0.19775
	0.5	−0.08143	0.06075	0.07764	0.9873
	1	−2.89297	2.78589	0.01232	0.98468
	1.5	1.49872	1.49872	−0.05247	0.97794

Turing patterns, i.e., the distribution of u_i. Simple functions, such as exponential functions, can be used to depict such correlations. Therefore, we may call these phenomena the exponential correlations induced by higher-order connections in simplicial complexes.

IV. DISCUSSION

We investigated the formation of Turing patterns in simplicial complexes and their associated properties. Unlike in traditional networks, a link in a simplicial complex can connect more than just two nodes. We have emphasized that in the absence of higher-order interactions the theory of networks fails to comprehensively describe group interactions, and that thus a paradigm shift is under way in network science where this is remedied by means of simplicial complexes [52]. In this light, it is therefore of significant interest to investigate the theory of Turing patterns in this new theoretical framework. We have thus developed a reaction-diffusion model that is embedded in simplicial complexes, and where higher-order connections support the diffusion between patches such that the transfer flux per unit time is correctly determined.

We have shown that there exist conditions where the presence of higher-order connections is a necessary condition for the emergence of Turing patterns. In other words, higher-order connections alone can be the trigger for the spontaneous emergence of spatiotemporal pattern formation, which has far-reaching implications for a variety of social, biological, and technological systems. Moreover, we have performed extensive simulations with three paradigmatic dynamical models that can be used to describe a reaction-diffusion process, and apart from the fact that Turing patterns can sometimes spontaneously emerge only if higher-order connections are present but not in the corresponding reduced "standard" network with pairwise connections, we have shown also that the structure of Turing patterns is strongly correlated with the average degree of higher-order connections in simplicial complexes.

Taken together, we here make an important step forward in the investigation of Turing patterns that arise from reaction-diffusion systems in higher-order networks, although several directions remain open for future research. In particular, it remains of interest to consider simplicial complexes with higher orders, as well as with distributions other than random, such as exponential random simplicial complexes [47,48] and scale-free simplicial complexes [49]. We hope that our results will prove inspirational to that effect and motivate future research of Turing patterns in higher-order networks.

ACKNOWLEDGMENTS

This work is supported by the National Natural Science Fund of Distinguished Young Scholarship of China (Grant No. 62025602), the National Natural Science Foundation of China (Grants No. U1803263, 11931015, 81961138010, 11975025), the Fok Ying-Tong Education Foundation, China (Grant No. 171105), the Technological Innovation Team of Shaanxi Province (No. 2020TD-013), and Fundamental Research Funds for the Central Universities (Grants No. D5000210738, D5000211001). M.P. was supported by the Slovenian Research Agency (Grants No. P1-0403 and J1-2457). We also acknowledge the XPLORER PRIZE.

APPENDIX A: TURING INSTABILITY CONDITION

The underlying topology where reaction-diffusion processes are defined plays a decisive role in the emergence of Turing patterns [29]. We give a detailed derivation of the Turing instability conditions in regard to the topology's Laplacian matrix. Let $f(u_i, v_i) = 0$ and $g(u_i, v_i) = 0$, we can get the equilibrium point (u^e, v^e). Adding small perturbations to the equilibrium point, we have

$$(u_i, v_i) = (u^e, v^e) + (\Delta u_i, \Delta v_i), \tag{A1}$$

substituting Eq. (A1) into Eq. (5) and carrying Taylor expansion of $f(u_i, v_i)$ and $g(u_i, v_i)$, we get

$$\begin{aligned}\frac{d\Delta u_i}{dt} &= f_u \Delta u_i + f_v \Delta v_i + \varepsilon \sum_{j=1}^{N} L_{ij} \Delta u_j,\\ \frac{d\Delta v_i}{dt} &= g_u \Delta u_i + g_v \Delta v_i + \sigma\varepsilon \sum_{j=1}^{N} L_{ij} \Delta v_j,\end{aligned} \tag{A2}$$

where f_u and f_v are the partial derivatives in regard to the equilibrium point (u^e, v^e) of $f(u_i, v_i)$. Similarly, g_u and g_v are the ones of $g(u_i, v_i)$. Then the perturbations are expanded as

$$\Delta u_i(t) = \sum_{\alpha=1}^{N} C_u^\alpha e^{\lambda_\alpha t} \phi_i^\alpha, \quad \Delta v_i(t) = \sum_{\alpha=1}^{N} C_v^\alpha e^{\lambda_\alpha t} \phi_i^\alpha, \tag{A3}$$

where ϕ_i^α is the ith entry of the eigenvector ϕ^α. Λ_α denotes the eigenvalue of L which corresponds to ϕ^α. Therefore

$$\sum_{j=1}^{N} L_{ij} \phi_j^\alpha = \Lambda_\alpha \phi_i^\alpha, \quad \alpha = 1, \ldots, N. \tag{A4}$$

By substituting Eqs. (A3) and (A4), Eq. (A2) turns to a equation about the linearized growth factor λ_α

$$\begin{bmatrix} \lambda_\alpha - f_u - \varepsilon\Lambda_\alpha & f_v \\ g_u & \lambda_\alpha - g_v - \sigma\varepsilon\Lambda_\alpha \end{bmatrix} \begin{bmatrix} C_u^\alpha \\ C_v^\alpha \end{bmatrix} = 0 \tag{A5}$$

whose characteristic equation is

$$\lambda_\alpha^2 - P(\Lambda_\alpha)\lambda_\alpha + Q(\Lambda_\alpha) = 0, \tag{A6}$$

where

$$\begin{aligned}P(\Lambda_\alpha) &= f_u + g_v + \varepsilon(1+\sigma)\Lambda_\alpha,\\ Q(\Lambda_\alpha) &= \sigma\varepsilon^2\Lambda_\alpha^2 + \varepsilon(g_v + \sigma f_u)\Lambda_\alpha + f_u g_v - f_v g_u.\end{aligned} \tag{A7}$$

Equation (A6) has two solutions:

$$\begin{aligned}\lambda_{\alpha_1} &= \frac{P(\Lambda_\alpha) + \sqrt{P(\Lambda_\alpha)^2 - 4Q(\Lambda_\alpha)}}{2},\\ \lambda_{\alpha_2} &= \frac{P(\Lambda_\alpha) - \sqrt{P(\Lambda_\alpha)^2 - 4Q(\Lambda_\alpha)}}{2}.\end{aligned} \tag{A8}$$

In line with the Turing theory, when there is no diffusion, the perturbations must reduce to zero, which requires

$$\begin{aligned}P(0) &= f_u + g_v < 0,\\ Q(0) &= f_u g_v - f_v g_u > 0,\end{aligned} \tag{A9}$$

and Eq. (A9) can be satisfied by adjusting model-specific parameters.

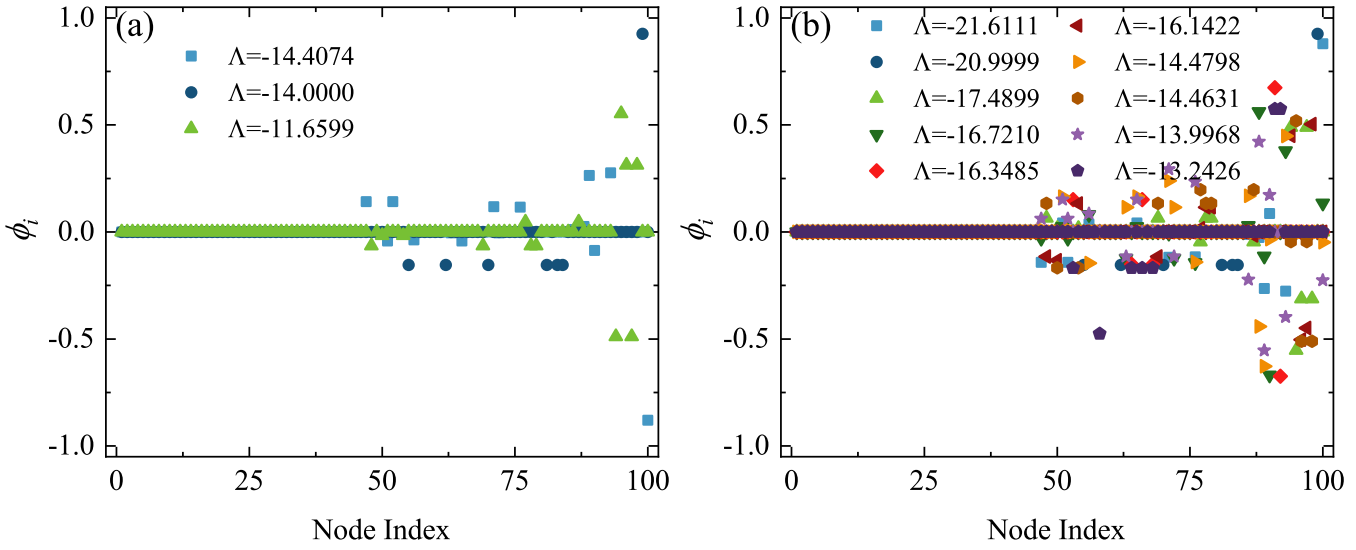

FIG. 8. The value distribution of critical eigenvectors corresponding to the unstable eigenvalues (the abscissa of the red points) in Figs. 4(b) and 4(c). There are three and ten eigenvalues unstable in Figs. 4(b) and 4(c), respectively. Panels (a) and (b) plot the value distribution of critical eigenvectors corresponding to the unstable eigenvalues in Figs. 4(b) and 4(c), respectively. It can be seen that only a subset of values are nonzero in both panels (a) and (b), which can explain that Turing patterns only develop on a subset of nodes in Figs. 4(b) and 4(c).

Moreover, Turing instability requires $\mathrm{Re}(\lambda_\alpha > 0)$ when diffusion is taken into account. Note that $P(\Lambda_\alpha) = P(0) + \varepsilon(1+\sigma)\Lambda_\alpha < 0$, because $P(0) < 0$ (as Turing instability requires when there is no diffusion) and $(1+\sigma)\Lambda_\alpha < 0$ (σ is a positive parameter and the eigenvalue of the Laplacian matrix is negative). Therefore only λ_{α_1} is possible to have positive real part. To ensure $\mathrm{Re}(\lambda_{\alpha_1}) > 0$, we demand that $Q(\Lambda_\alpha) < 0$:

$$Q(\Lambda_\alpha) = \sigma\varepsilon^2\Lambda_\alpha^2 + \varepsilon(g_v + \sigma f_u)\Lambda_\alpha + f_u g_v - f_v g_u < 0. \tag{A10}$$

Solving the equation $Q(\Lambda_\alpha) = 0$, we get the following solutions:

$$\Lambda^* = \frac{-(g_v + f_u\sigma) + \sqrt{(g_v+\sigma f_u)^2 - 4\sigma(f_u g_v - f_v g_u)}}{2\sigma\varepsilon},$$
$$\Lambda^{**} = \frac{-(g_v + f_u\sigma) - \sqrt{(g_v+\sigma f_u)^2 - 4\sigma(f_u g_v - f_v g_u)}}{2\sigma\varepsilon}. \tag{A11}$$

Given that σ and ε are parameters with positive values, $Q(\Lambda_\alpha)$ is then a quadratic function of Λ_α with openings upwards. Therefore, when Λ_α is in the range $(\Lambda^*, \Lambda^{**})$, the condition $Q(\Lambda_\alpha) < 0$ is satisfied. Hence, the topology will meet the Turing instability condition if its Laplacian matrix has eigenvalues located in the range $(\Lambda^*, \Lambda^{**})$.

APPENDIX B: TURING PATTERNS INDUCED BY HIGHER-ORDER CONNECTIONS

Figure 8 shows the value distribution of eigenvectors that correspond to the critical mode in Figs. 4(b) and 4(c), explaining why only a subset of nodes deviate from the equilibrium in the stationary Turing patterns.

Similar to the results in Fig. 4 for the GM model in the main text, the phenomenon that Turing patterns can be induced by higher-order connections is also found in the LG (Fig. 9) and FHN (Fig. 10) models. Figure 11 shows the bifurcation diagrams of the LG and FHN models, supporting the claim in Figs. 9 and 10 that Turing patterns can be induced by higher-order connections for the LG and FHN models.

APPENDIX C: MEAN-FIELD ANALYSIS OF TURING PATTERNS ON SIMPLICIAL COMPLEXES

Following the theory proposed by Nakao and Mikhailov [30], we establish the mean-field approximation for the reaction-diffusion model on simplicial complexes. First, the equation (5) can be rewritten as

$$\frac{du_i}{dt} = f(u_i, v_i) + \varepsilon\left(h_i^{(u)} - k_i u_i\right),$$
$$\frac{dv_i}{dt} = g(u_i, v_i) + \sigma\varepsilon\left(h_i^{(v)} - k_i v_i\right), \tag{C1}$$

where $h_i^{(u)} = \sum_{j=1}^N A_{ij}u_j$ and $h_i^{(v)} = \sum_{j=1}^N A_{ij}v_j$ are the local fields perceived by each node. These local fields can be approximated as $h_i^{(u)} \approx k_i H^{(u)}$ and $h_i^{(v)} \approx k_i H^{(v)}$, where $H^{(u)} = \sum_{j=1}^N w_j u_j$ and $H^{(v)} = \sum_{j=1}^N w_j v_j$ are global mean fields. The weights $w_j = k_j/(\sum_{l=1}^N k_l)$ account for the varying contributions made by each node to the global mean field.

According to this approximation, we have the following dynamics characterized by the global mean fields:

$$\frac{du_i}{dt} = f(u_i, v_i) + \varepsilon k_i(H^{(u)} - u_i),$$
$$\frac{dv_i}{dt} = g(u_i, v_i) + \sigma\varepsilon k_i(H^{(v)} - v_i). \tag{C2}$$

In the system characterized by (C2), the activator and inhibitor in each node only interact with the global mean fields $H^{(u)}$ and $H^{(v)}$ instead of the the activator and inhibitor in other nodes.

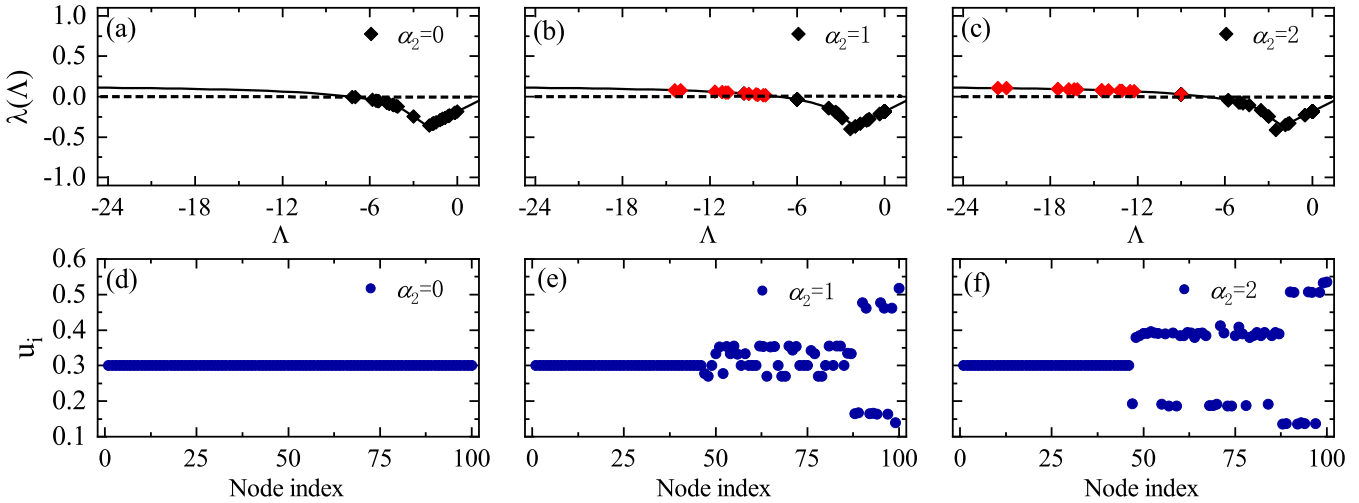

FIG. 9. Turing patterns induced by three-body connections (2-simplices) for LG model. Panels (a), (b), and (c) respectively show the dispersion relationship between the system growth factor λ and Laplacian eigenvalue Λ for $\alpha_2 = 0$, 1, and 2. The simplicial complex used here is the same as the one used in Fig. 3. The 1-simplex strength α_1 is fixed to 1. The dispersion curve is calculated through Turing instability analysis. Turing patterns will arise only if Laplacian eigenvalues meet the condition that $\exists\Lambda$, $\lambda(\Lambda) > 0$. Panels (d), (e), and (f) then respectively present the corresponding distributions of u_i after numerical calculations for $\alpha_2 = 0$, 1, and 2. $\alpha_2 = 0$ implies that the simplicial complex returns to a "standard" network. When $\alpha_2 = 0$, the Turing instability condition is not satisfied (a), resulting in a homogeneous distribution of u_i (d). Interestingly, when $\alpha_2 > 0$, such as $\alpha_2 = 1, 2$, the three-body connections are taken into account, the Turing instability condition is satisfied as shown in panels (b) and (c). The dispersion points that meet the instability requirement are colored in red in panels (b) and (c). Panels (e) and (f) then exhibit the corresponding distributions of u_i as Turing patterns for $\alpha_2 = 1, 2$.

In Fig. 7 we first calculate the global mean fields $H^{(u)}$ and $H^{(v)}$ according to the stationary Turing patterns (the stable heterogeneous distribution of u_i) obtained by numerically solving Eq. (5). We then can solve Eq. (C2) with specific global mean fields $H^{(u)}$ and $H^{(v)}$.

APPENDIX D: DETAILED INFORMATION FOR THE NONLINEAR REGRESSION FITTING

The detailed information for the nonlinear regression fitting curves of results obtained by numerical simulations and mean-field analysis in Fig. 7 is shown in Tables I and II.

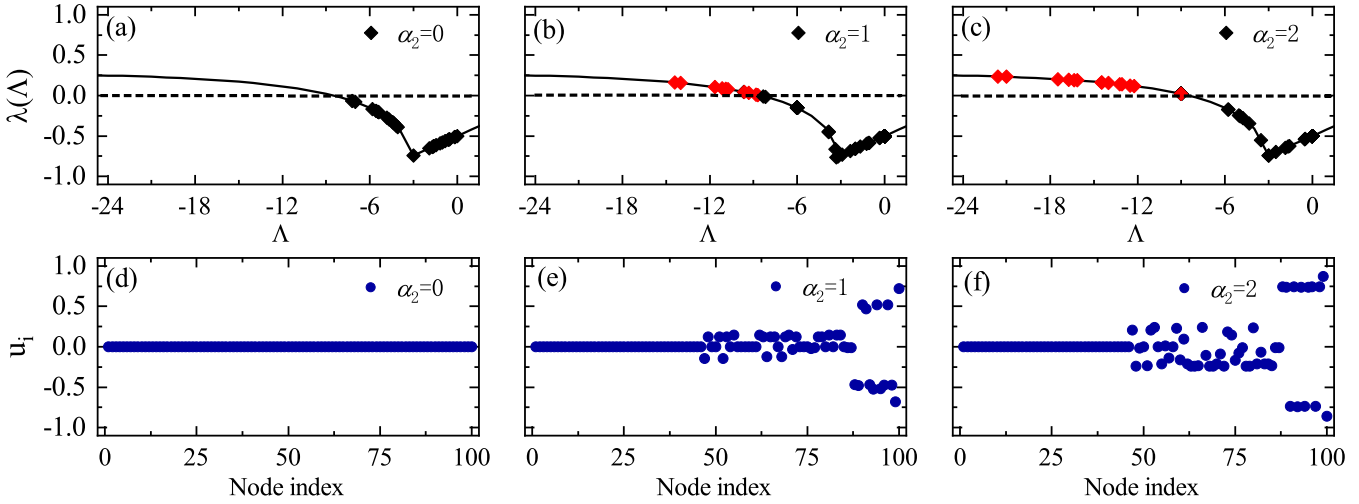

FIG. 10. Turing patterns induced by three-body connections (2-simplices) for FHN model. Panels (a), (b), and (c) respectively show the dispersion relationship between the system growth factor λ and Laplacian eigenvalue Λ for $\alpha_2 = 0$, 1, and 2. The simplicial complex used here is the same as the one used in Fig. 3. The 1-simplex strength α_1 is fixed to 1. The dispersion curve is calculated through Turing instability analysis. Turing patterns will arise only if Laplacian eigenvalues meet the condition that $\exists\Lambda$, $\lambda(\Lambda) > 0$. Panels (d), (e), and (f) then respectively present the corresponding distributions of u_i after numerical calculations for $\alpha_2 = 0$, 1, and 2. $\alpha_2 = 0$ implies that the simplicial complex returns to a "standard" network. When $\alpha_2 = 0$, the Turing instability condition is not satisfied (a), resulting in a homogeneous distribution of u_i (d). Interestingly, when $\alpha_2 > 0$, such as $\alpha_2 = 1, 2$, the three-body connections are taken into account, the Turing instability condition is satisfied as shown in panels (b) and (c). The dispersion points that meet the instability requirement are colored in red in panels (b) and (c). Panels (e) and (f) then exhibit the corresponding distributions of u_i as Turing patterns for $\alpha_2 = 1, 2$.

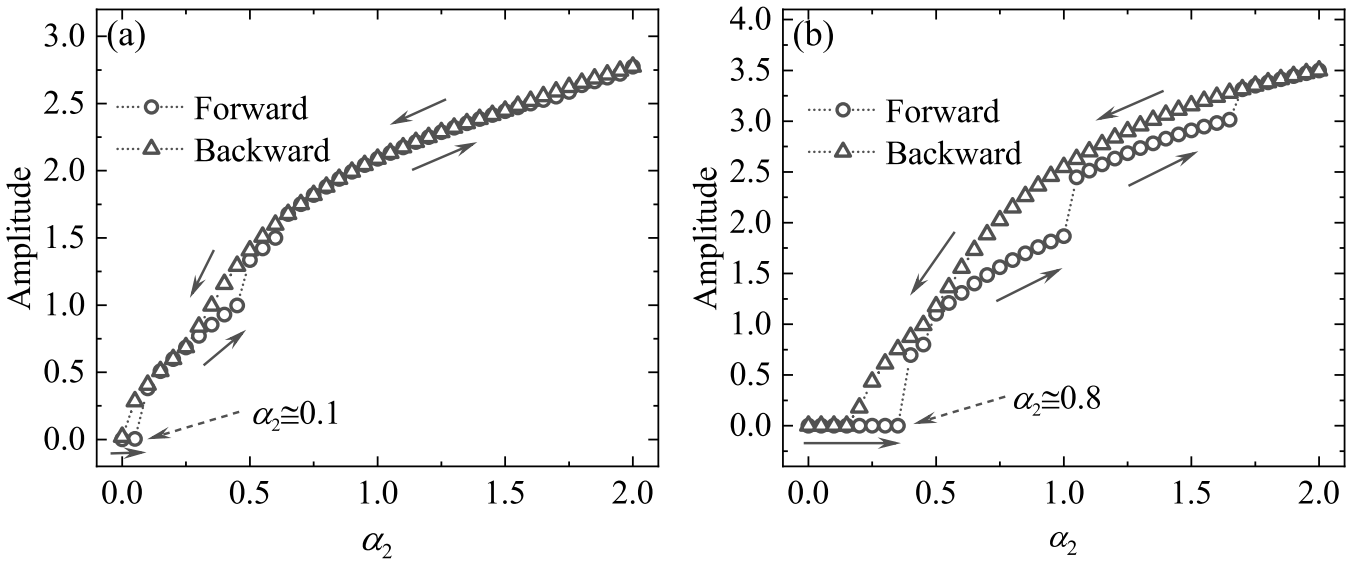

FIG. 11. Multistabilities of the LG (a) and FHN (b) models on simplicial complexes. The amplitude of the solutions under varying α_2 in either an upward or downward direction is plotted vs the 2-simplex strength α_2. Starting to increase α_2 from 0 with the initial condition (11), the amplitude goes through a sudden jump from 0 at $\alpha_2 \cong 0.1$ (the LF model) and $\alpha_2 \cong 0.8$ (the FHN model). Further changing the value of α_2, the coexistence of multiple stable solutions and hysteresis can be observed. The changing direction of α_2 is directed by arrows. The simplicial complex used here is the same as the one used in Figs. 3 and 4.

[1] A. M. Turing, The chemical basis of morphogenesis, Philos. Trans. R. Soc. Lond. B **237**, 37 (1952).

[2] A. Gierer and H. Meinhardt, A theory of biological pattern formation, Kybernetik **12**, 30 (1972).

[3] S. Kondo and T. Miura, Reaction-diffusion model as a framework for understanding biological pattern formation, Science **329**, 1616 (2010).

[4] A. Nakamasu, G. Takahashi, A. Kanbe, and S. Kondo, Interactions between zebrafish pigment cells responsible for the generation of Turing patterns, Proc. Natl. Acad. Sci. USA **106**, 8429 (2009).

[5] S. Hata, H. Nakao, and A. S. Mikhailov, Dispersal-induced destabilization of metapopulations and oscillatory Turing patterns in ecological networks, Sci. Rep. **4**, 3585 (2014).

[6] N. P. Taylor, H. Kim, A. L. Krause, and R. A. Van Gorder, A non-local cross-diffusion model of population dynamics I: Emergent spatial and spatiotemporal patterns, Bull. Math. Biol. **82**, 112 (2020).

[7] Y. Fuseya, H. Katsuno, K. Behnia, and A. Kapitulnik, Nanoscale Turing patterns in a bismuth monolayer, Nat. Phys. **17**, 1031 (2021).

[8] M. B. Short, A. L. Bertozzi, and P. J. Brantingham, Nonlinear patterns in urban crime: Hotspots, bifurcations, and suppression, SIAM J. Appl. Dyn. Syst. **9**, 462 (2010).

[9] J. Y. Wakano, M. A. Nowak, and C. Hauert, Spatial dynamics of ecological public goods, Proc. Natl. Acad. Sci. USA **106**, 7910 (2009).

[10] V. K. Vanag and I. R. Epstein, Pattern Formation in a Tunable Medium: The Belousov-Zhabotinsky Reaction in an Aerosol ot Microemulsion, Phys. Rev. Lett. **87**, 228301 (2001).

[11] Z. Tan, S. Chen, X. Peng, L. Zhang, and C. Gao, Polyamide membranes with nanoscale Turing structures for water purification, Science **360**, 518 (2018).

[12] P. K. Grant, N. Dalchau, J. R. Brown, F. Federici, T. J. Rudge, B. Yordanov, O. Patange, A. Phillips, and J. Haseloff, Orthogonal intercellular signaling for programmed spatial behavior, Mol. Syst. Biol. **12**, 849 (2016).

[13] C. R. Boehm, P. K. Grant, and J. Haseloff, Programmed hierarchical patterning of bacterial populations, Nat. Commun. **9**, 776 (2018).

[14] D. Karig, K. M. Martini, T. Lu, N. A. DeLateur, N. Goldenfeld, and R. Weiss, Stochastic Turing patterns in a synthetic bacterial population, Proc. Natl. Acad. Sci. USA **115**, 6572 (2018).

[15] M. G. Neubert, H. Caswell, and J. D. Murray, Transient dynamics and pattern formation: Reactivity is necessary for Turing instabilities, Math. Biosci. **175**, 1 (2002).

[16] T. Bánsági, V. K. Vanag, and I. R. Epstein, Tomography of reaction-diffusion microemulsions reveals three-dimensional Turing patterns, Science **331**, 1309 (2011).

[17] H. Hu, Q. Li, and S. Li, Traveling and standing patterns induced by delay feedback in uniform oscillatory reaction–diffusion system, Chem. Phys. Lett. **447**, 364 (2007).

[18] I. Lengyel and I. R. Epstein, A chemical approach to designing Turing patterns in reaction-diffusion systems, Proc. Natl. Acad. Sci. USA **89**, 3977 (1992).

[19] H. Levine and W. Rappel, Membrane-bound Turing patterns, Phys. Rev. E **72**, 061912 (2005).

[20] A. Marciniak-Czochra, G. Karch, and K. Suzuki, Instability of Turing patterns in reaction-diffusion-ode systems, J. Math. Biol. **74**, 583 (2017).

[21] Q. Ouyang and H. L. Swinney, Transition from a uniform state to hexagonal and striped Turing patterns, Nature (London) **352**, 610 (1991).

[22] B. Peña and C. Pérez-García, Stability of Turing patterns in the Brusselator model, Phys. Rev. E **64**, 056213 (2001).

[23] C. Varea, J. L. Aragón, and R. A. Barrio, Turing patterns on a sphere, Phys. Rev. E **60**, 4588 (1999).
[24] T. Zhang and H. Zang, Delay-induced Turing instability in reaction-diffusion equations, Phys. Rev. E **90**, 052908 (2014).
[25] M. Asslani, F. Di Patti, and D. Fanelli, Stochastic Turing patterns on a network, Phys. Rev. E **86**, 046105 (2012).
[26] L. Chang, C. Liu, G. Sun, Z. Wang, and Z. Jin, Delay-induced patterns in a predator-prey model on complex networks with diffusion, New J. Phys. **21**, 073035 (2019).
[27] L. D. Fernandes and M. A. M. de Aguiar, Turing patterns and apparent competition in predator-prey food webs on networks, Phys. Rev. E **86**, 056203 (2012).
[28] S. Hata, H. Nakao, and A. S. Mikhailov, Global feedback control of Turing patterns in network-organized activator-inhibitor systems, Europhys. Lett. **98**, 64004 (2012).
[29] S. Mimar, M. M. Juane, J. Park, A. P. Muñuzuri, and G. Ghoshal, Turing patterns mediated by network topology in homogeneous active systems, Phys. Rev. E **99**, 062303 (2019).
[30] H. Nakao and A. S. Mikhailov, Turing patterns in network-organized activator–inhibitor systems, Nat. Phys. **6**, 544 (2010).
[31] H. G. Othmer and L. E. Scriven, Instability and dynamic pattern in cellular networks, J. Theor. Biol. **32**, 507 (1971).
[32] M. Asllani, J. D. Challenger, F. S. Pavone, L. Sacconi, and D. Fanelli, The theory of pattern formation on directed networks, Nat. Commun. **5**, 4517 (2014).
[33] W. Horsthemke, K. Lam, and P. K. Moore, Network topology and Turing instabilities in small arrays of diffusively coupled reactors, Phys. Lett. A **328**, 444 (2004).
[34] P. K. Moore and W. Horsthemke, Localized patterns in homogeneous networks of diffusively coupled reactors, Physica D **206**, 121 (2005).
[35] H. G. Othmer and L. E. Scriven, Non-linear aspects of dynamic pattern in cellular networks, J. Theor. Biol. **43**, 83 (1974).
[36] M. Asllani, D. M. Busiello, T. Carletti, D. Fanelli, and G. Planchon, Turing patterns in multiplex networks, Phys. Rev. E **90**, 042814 (2014).
[37] N. E. Kouvaris, S. Hata, and A. Guilera, Pattern formation in multiplex networks, Sci. Rep. **5**, 10840 (2015).
[38] S. Gao, L. Chang, X. Wang, C. Liu, X. Li, and Z. Wang, Cross-diffusion on multiplex networks, New J. Phys. **22**, 053047 (2020).
[39] J. Petit, B. Lauwens, D. Fanelli, and T. Carletti, Theory of Turing Patterns on Time Varying Networks, Phys. Rev. Lett. **119**, 148301 (2017).
[40] R. A. Van Gorder, A theory of pattern formation for reaction–diffusion systems on temporal networks, Proc. R. Soc. Math. Phys. Eng. Sci. **477**, 20200753 (2021).
[41] R. Muolo, M. Asllani, D. Fanelli, P. K. Maini, and T. Carletti, Patterns of non-normality in networked systems, J. Theor. Biol. **480**, 81 (2019).
[42] I. Iacopini, G. Petri, A. Barrat, and V. Latora, Simplicial models of social contagion, Nat. Commun. **10**, 2485 (2019).
[43] F. Battiston, G. Cencetti, I. Iacopini, V. Latora, M. Lucas, A. Patania, J. G. Young, and G. Petri, Networks beyond pairwise interactions: Structure and dynamics, Phys. Rep. **874**, 1 (2020).
[44] T. Carletti, F. Battiston, G. Cencetti, and D. Fanelli, Random walks on hypergraphs, Phys. Rev. E **101**, 022308 (2020).
[45] G. Chao, Z. Junzhou, Z. Fan, W. Zhen, and L. Xuelong, A novel representation learning for dynamic graphs based on graph convolutional networks, IEEE Trans. Cybern. **1**, 1 (2022).
[46] T. Carletti, D. Fanelli, and S. Nicoletti, Dynamical systems on hypergraphs, J. Phys. Complex. **1**, 035006 (2020).
[47] O. T. Courtney and G. Bianconi, Generalized network structures: The configuration model and the canonical ensemble of simplicial complexes, Phys. Rev. E **93**, 062311 (2016).
[48] O. T. Courtney and G. Bianconi, Weighted growing simplicial complexes, Phys. Rev. E **95**, 062301 (2017).
[49] K. Kovalenko, I. Sendiña-Nadal, N. Khalil, A. Dainiak, D. Musatov, A. M. Raigorodskii, K. Alfaro-Bittner, B. Barzel, and S. Boccaletti, Growing scale-free simplices, Commun. Phys. **4**, 43 (2021).
[50] U. Alvarez-Rodriguez, F. Battiston, G. F. de Arruda, Y. Moreno, M. Perc, and V. Latora, Evolutionary dynamics of higher-order interactions in social networks, Nat. Hum. Behav. **5**, 586 (2022).
[51] A. Kumar, S. Chowdhary, V. Capraro, and M. Perc, Evolution of honesty in higher-order social networks, Phys. Rev. E **104**, 054308 (2021).
[52] G. Bianconi, *Higher-Order Networks: An Introduction to Simplicial Complexes* (Cambridge University Press, Cambridge, 2021).
[53] S. Majhi, M. Perc, and D. Ghosh, Dynamics on higher-order networks: A review, J. R. Soc. Interface **19**, 20220043 (2022).
[54] P. H. Leslie and J. C. Gower, The properties of a stochastic model for the predator-prey type of interaction between two species, Biometrika **47**, 219 (1960).
[55] C. Liu, L. Chang, Y. Huang, and Z. Wang, Turing patterns in a predator–prey model on complex networks, Nonlinear Dyn. **99**, 3313 (2020).
[56] C. Wang, L. Chang, and H. Liu, Spatial patterns of a predator-prey system of Leslie type with time delay, PLoS ONE **11**, e0150503 (2016).
[57] R. FitzHugh, Impulses and physiological states in theoretical models of nerve membrane, Biophys. J. **1**, 445 (1961).
[58] J. Nagumo, S. Arimoto, and S. Yoshizawa, An active pulse transmission line simulating nerve axon, Proc. IRE **50**, 2061 (1962).
[59] Z. Qianqian, S. Jianwei, and X. Yong, Turing instability in the reaction-diffusion network, Phys. Rev. E **102**, 062215 (2020).
[60] T. Carletti and H. Nakao, Turing patterns in a network-reduced FitzHugh-Nagumo model, Phys. Rev. E **101**, 022203 (2020).